

# Experimental realization of quantum non-reciprocity based on cold atomic ensembles

Ming-Xin Dong,<sup>1,2</sup> Yi-Chen Yu,<sup>1,2</sup> Ying-Hao Ye,<sup>1,2</sup> Wei-Hang Zhang,<sup>1,2</sup> En-Ze Li,<sup>1,2</sup> Lei Zeng,<sup>1,2</sup> Guang-Can Guo,<sup>1,2</sup> Dong-Sheng Ding,<sup>1,2,\*</sup> and Bao-Sen Shi<sup>1,2,†</sup>

<sup>1</sup>Key Laboratory of Quantum Information, University of Science and Technology of China, Hefei, Anhui 230026, China.

<sup>2</sup>Synergetic Innovation Center of Quantum Information and Quantum Physics, University of Science and Technology of China, Hefei, Anhui 230026, China.

(Dated: August 27, 2019)

In analog to counterparts widely used in electronic circuits, all optical non-reciprocal devices are basic building blocks for both classical and quantum optical information processing. Approaching the fundamental limit of such devices, where the propagation of a single photon exhibits a good non-reciprocal characteristic, requires an asymmetric strong coupling between a single photon and a matter. Unfortunately it has been not realized yet. Here, we propose and experimentally realize a quantum non-reciprocity device with low optical losses and a high isolation of larger than 14 dB based on the cold atoms. Besides, the non-reciprocal transmission of a quantum qubit and non-reciprocal quantum storage of a true single photon are also realized. All results achieved would be very promising in building up quantum non-reciprocal devices for quantum networks.

Non-reciprocal devices, such as circulators and isolators used for indispensable components in information processing, no matter in electronic circuits, or in quantum networks, have attracted a lot of attentions. Optical non-reciprocal devices, as for optical-based functional components controlling the flow of light, are crucial for advanced optical communication and quantum information processing [1, 2]. To achieve an optical non-reciprocal device, ones have to break Lorentz reciprocity [3, 4]. Motivated by the desirable applications in on-chip integration system and quantum networks, a variety of methods with distinct physical principles have been proposed to realize optical non-reciprocity. One approach is using the spatio-temporal modulation [5–10] of the permittivity of nonlinear materials to break time-reversal symmetry. An alternative approach is to use nonlinear processes to construct a nonlinear optical isolation [11–14]. In addition, many other schemes have been proposed based on various systems, such as opto-mechanical system [15–21], atomic system [22–26] and chiral quantum optics system [2, 27–31].

To date, most of reported schemes have been performed with a weak coherent light. However, many practical quantum information processes require a genuine single photon, not a weak coherent pulse, such as linear quantum computation[32]. Hence, the ability of realizing single-photon non-reciprocity is a basic require-

ment for a quantum network. Nowadays, many feasible schemes have been proposed to realize single photon non-reciprocity [33–37], for example, very recently, Liu et al. proposed a possible experimental scheme to implement phase controlled single-photon non-reciprocal transmission based on an one-dimensional waveguide [37]. However, the single photon non-reciprocity has not been realized yet. The experimental realization of a true single-photon non-reciprocity is always the focus of people’s attentions for potential applications in quantum network such as constructing a quantum transistor [38] and quantum router [34], therefore it is desirable and also a big challenge to experimentally realize non-reciprocity in full quantum regime.

Here, we propose and experimentally realize a scheme to achieve a true single-photon non-reciprocity in a cold atomic ensemble. The underlying physics in our scheme is the asymmetric coupling between a single photon and the specific atomic transition, which results in an asymmetric permittivity and break the Lorentz reciprocity. We use a heralded single photon to demonstrate quantum non-reciprocity with low optical losses and high isolation. Moreover, the proof-of-principle experimental demonstration of non-reciprocal transmission of an arbitrary polarized qubit and non-reciprocal quantum storage of a true single photon are also realized. We believe all results are very promising for non-reciprocal quantum information processing.

In the experimental diagram, a pair of non-classical correlated photons called Stokes and anti-Stokes photon (labeled as S1 and S2) are emitted through spontaneously four-wave mixing (SFWM) [39, 40] process in atomic cloud 1 (the optical depth ( $OD$ ) is 14), as shown in the top part in Fig.1(a). Two pump beams called pump 1 (780 nm, Rabi frequency  $2\pi \times 0.67$  MHz) and pump 2 (795 nm, Rabi frequency  $2\pi \times 4.84$  MHz) with orthogonal circularly polarization counter-propagate through the atomic cloud 1. The photons S1 and S2 are collected at an angle of  $3^\circ$  with respect to the pump lasers. S1 photon is detected by a single photon counting module, the heralded single photon S2 is collected and then coupled into a single-mode fiber for the demonstration of quantum non-reciprocity. Subsequently, we input S2 photon into the atomic cloud 2 from port 1 and port 2 respectively and study the transmission properties of the corresponding output ports as shown in the bottom part in Fig.1(a).

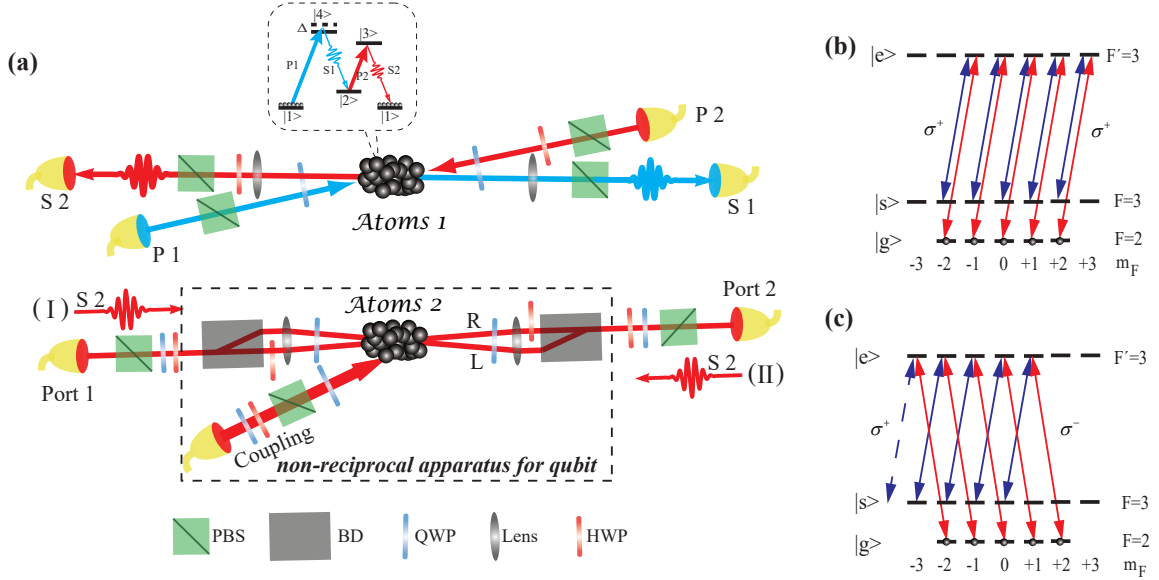


Figure 1. **Experimental realization of quantum-regime non-reciprocity.** (a) Schematic diagram of experimental setup. Upper layer of setup is used to generate a heralded single photon through SFWM process in the cold atomic cloud 1 and the relevant energy level configuration shown in the dashed-line rounded rectangle.  $\Delta$  represents the detuning of pump 1, which is set to be  $2\pi \times 50$  MHz.  $|1\rangle = |5S_{1/2}, F=2\rangle$ ,  $|2\rangle = |5S_{1/2}, F=3\rangle$ ,  $|3\rangle = |5P_{1/2}, F'=3\rangle$  and  $|4\rangle = |5P_{3/2}, F'=3\rangle$ . The lower layer is utilized to demonstrate the quantum non-reciprocity, including a non-reciprocal apparatus for a qubit as depicted in the dashed-line rectangle. (b) The exploited multi-Zeeman sub-levels configuration in the forward-propagation case. Signal field is  $\sigma^+$  polarized and coupling laser is  $\sigma^+$  polarized that both propagate in the forward direction. The states  $|g\rangle$ ,  $|s\rangle$ ,  $|e\rangle$  correspond to  $|1\rangle$ ,  $|2\rangle$ ,  $|3\rangle$  respectively. (c) The multi-Zeeman sub-levels configuration in the backward-propagation case, and signal field is  $\sigma^-$  polarized that propagates in the backward direction.

Here, the forward-propagation (backward-propagation) case I (II) is defined as the propagation of S2 photon from port 1 (2) to port 2 (1) while S2 photon co-propagates (counter-propagates) with coupling laser. The marked non-reciprocal apparatus for a qubit (NRAQ) shown in dotted square frame can be considered as a whole setup to realize quantum non-reciprocity, it is actually an optical isolation of a two-port device. The NRAQ mainly consists of the atomic cloud 2, a coupling laser and a pair of beam displacers (BDs). Here, we input the coupling laser into the atomic cloud 2 at an angle of  $2.8^\circ$  with the respect to the propagation direction of signal photon S2. In order to minimize the noise scattering from the coupling laser, we insert two home-made Fabry-Perot (FP) etalons (50% transmittance, 500 MHz bandwidth) for frequency filtering before the single photon detectors.

Fig. 1(b), (c) depict the relevant energy-level configurations in forward-propagation and backward-propagation cases, where the signal (red) and coupling (blue) fields couple corresponding atomic levels respectively.  $m_F$  is the magnetic quantum number of the atomic hyperfine states and the  $\sigma^+/\sigma^-$  polarized signal photon couples the atomic transition  $\Delta m_F = +1/-1$  respectively. We take into account all degenerate Zeeman sublevels in theoretical analysis [41, 42]. In Fig. 1(b), the five Zeeman transitions for signals (red lines) are all connected with

the coupling transitions, which can be treated as an effectively completed  $\Lambda$ -type electromagnetically induced transparency (EIT) system [43], thereby the atoms initially populated in  $|g\rangle$  are transparent for the forward-propagated photons due to the quantum interference effect. By comparison, for backward-propagation case depicted in Fig. 1(c), the transition of  $|g, m_F = -2\rangle \rightarrow |e, m_F = -3\rangle$  contributes to the absorption (see Method) which prevents the propagation of photons in backward direction. This renders asymmetric interaction between  $\sigma^+/\sigma^-$  polarized photons and atoms, causing the chirality in our system which can be exploited to realize quantum non-reciprocity.

At first, we study the single-photon non-reciprocity, in this case we block one optical path  $L$  after signal S2 passes through a BD in Fig. 1(a). The measured single-photon wave packets with a resolution of 1.6 ns for forward-propagation (red line) and backward-propagation cases (blue line) are depicted in Fig. 2(a) respectively. Here, we select a suitable temporal length of S2 photon matching the EIT bandwidth of the atomic cloud 2 to obtain the maximum transmission rate in forward propagation case. The bandwidth of signal 2 is set to be  $2\pi \times 1.60$  MHz, which can be controlled by the Rabi frequency of pump 2. Moreover, according to Eq. 10 given in Method section, we should choose a suitable  $OD$

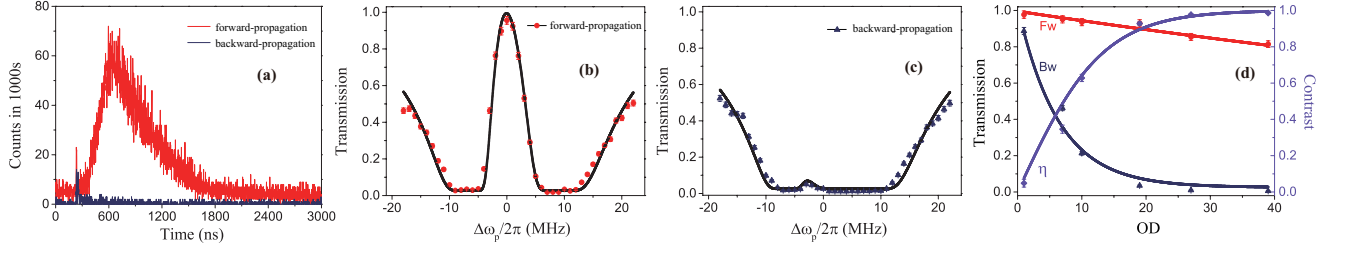


Figure 2. **Experimental results of single-photon non-reciprocity.** (a) The measured single photon wave packets for forward-propagation (red line) and backward-propagation (blue line) cases. (b) Single-photon EIT transmission spectra as a function of detuning from atomic resonance  $|g\rangle \rightarrow |e\rangle$  in forward-propagation case. The black line is the theoretical fitting. (c) Single-photon transmission versus detuning in backward-propagation case and black line is the theoretical fitting. (d) The transmissions FW (red), BW (blue) and contrast  $\eta$  (purple) as a function of  $OD$ . Here, FW (BW) refers to the forward-propagation (backward-propagation) case. The solid lines are the theoretical fittings by using Eq.10. The experiment and theory agreed well.

of the atomic cloud 2 and Rabi frequency of coupling laser to obtain high transmission and high isolation simultaneously. The  $OD$  of atomic cloud 2 is set to be 19, which is sufficient to prevent signal's propagation in the backward direction. Meanwhile, the Rabi frequency of coupling laser is set to be  $2.5\Gamma$  ( $\Gamma$  is the decay of level  $|3\rangle$ ), satisfying the requirement of high transmission in forward direction.

In the forward propagation case, the transmission rate is estimated to be 92.9%. By contrast, the transmission rate is near zero exhibiting a high isolation in backward propagation case. In addition, we define a contrast  $\eta$  between two propagation cases described by the following formula

$$\eta = \frac{CC_{fw} - CC_{bw}}{CC_{fw} + CC_{bw}} \quad (1)$$

where  $CC_{fw}/CC_{bw}$  represents the total integral coincidence counts in forward propagation/backward propagation case. The obtained  $\eta$  is 0.96, implying a sharp contrast between two propagation cases, this clearly characterizes a strong non-reciprocity in our scheme.

Subsequently, we explore the relation between the transmission and the frequency of signal 2 in two propagation cases. In the forward-propagation case, we obtain a single-photon EIT spectrum via changing the detuning of S2 photon from  $-2\pi \times 18 \sim +2\pi \times 22$  MHz as depicted in Fig.2(b). Here, the frequency detuning of S2 photon is achieved by varying the frequency of P2 laser controlled by an acousto-optic modulator (AOM). Accordingly, we observe a single photon transmission spectra as shown in Fig.2(c) in the backward-propagation case. Obviously, a high contrast is available as long as the single photons is resonant with the atomic transition of  $|g\rangle \rightarrow |e\rangle$ . In Fig.2(d), we plot the transmissions for forward propagation (red), backward propagation (blue) and the contrast  $\eta$  (purple) as a function of  $OD$ . When the  $OD$  is close to zero, the transmission becomes symmetric due to the

nearly identical transmissions in two propagation cases resulting in the vanish of non-reciprocal behavior. We could increase the isolation rate by increasing  $OD$  to obtain a better non-reciprocity.

Next, we characterize the transmission of qubits by inputting four polarization states  $|H\rangle$ ,  $|V\rangle$ ,  $|R\rangle = (|H\rangle - i|V\rangle)/\sqrt{2}$  and  $|D\rangle = (|H\rangle + |V\rangle)/\sqrt{2}$  into our non-reciprocal apparatus. The preparation of an arbitrary polarization qubit state of  $|\psi\rangle = \cos\frac{\theta}{2}|H\rangle + e^{i\phi}\sin\frac{\theta}{2}|V\rangle$  could be achieved by adjusting a quarter-wave plate (QWP) and a half-wave plate (HWP). Here,  $\theta$  and  $\phi$  represent the angle of HWP and QWP respectively. As sketched in Fig.1(a), the NRAQ is a spatially multiplexed dual-rail geometry constructed by a pair of BDs. We exploit BDs to spatially separate two orthogonal polarization components of qubits which transmit simultaneously in NRAQ. In addition, before signals enter into the atomic cloud 2, we make two components have identical circular polarization  $\sigma^+$  for satisfying the non-reciprocity conditions described in the above context. Hence, we insert a HWP on optical path  $R$  to convert the polarization of the photon from vertical to horizontal and a common QWP on both optical paths ( $L$  and  $R$ ) to convert the polarization of photon from horizontal to circular. Subsequently, the signals are focused into the centre of atoms by a lens with a focal length of 300 mm. Symmetrically, we recombine two paths into a single spatial mode with the assistance of a QWP, lens, HWP, and BD. Here, a pair of BDs form a long-time and passively-stabilized Mach-Zehnder (M-Z) interferometer and the relative phase between  $L$  and  $R$  is set to be zero by adjusting the tilt of BDs. In our experiment, we utilize two non-reciprocal processes simultaneously in a single NRAQ to realize non-reciprocal transmission of qubits. Ultimately, a polarization analyzer consisting of a QWP, HWP and PBS is exploited to measure the output state. For forward-propagation case, we characterize the output polarized states by using the quantum state tomography (see Method sections) and the reconstructed

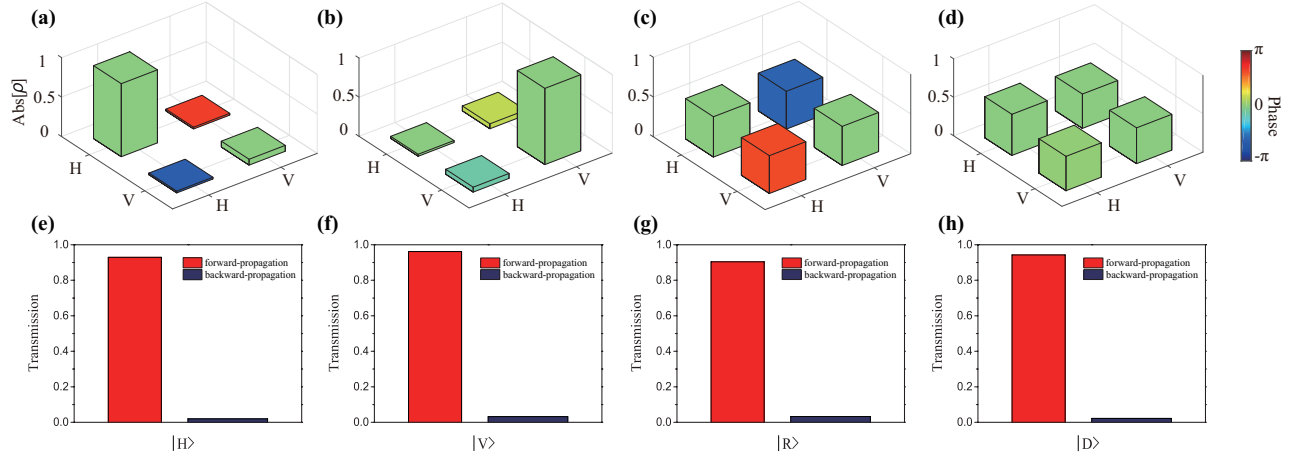


Figure 3. **The non-reciprocity for polarization qubits.** (a-d) The reconstructed density matrices for single photons encoded in  $|H\rangle$ ,  $|V\rangle$ ,  $|R\rangle$  and  $|D\rangle$  polarization respectively in the forward-propagation case. The height of bars denotes the magnitude  $\text{Abs}[\rho]$  and color represents phase. (e-h) The contrast of forward-propagation and backward-propagation cases for four polarization qubits.

**Table 1 | Transmission and isolation for single-photon polarization qubits**

$ \Psi\rangle$	Transmission rate	Transmission fidelity (%)	Isolation (dB)
$ H\rangle$	$0.9292 \pm 0.0239$	$92.64 \pm 0.69$	$17.12 \pm 0.11$
$ V\rangle$	$0.9619 \pm 0.0253$	$97.49 \pm 0.39$	$14.95 \pm 0.11$
$ R\rangle$	$0.9042 \pm 0.0239$	$93.85 \pm 0.76$	$14.86 \pm 0.12$
$ D\rangle$	$0.9427 \pm 0.0242$	$94.44 \pm 0.98$	$16.56 \pm 0.12$

density matrices are shown in Fig.3(a-d). By comparison, we measure the transmission in backward (blue) and forward directions (red) for four polarization qubit states as shown in Fig.3(e-h). It is obvious that we can observe high contrasts of 0.96, 0.94, 0.93, 0.95 respectively for four polarized states according to Eq.1.

To further quantify the performance of the NRQA, we have defined several parameters such as transmission rate, transmission fidelity for forward propagation case and isolation for backward propagation case. Here, the transmission fidelity  $\mathcal{F}$  is defined in Method sections, and the transmission rate  $T_{\text{fw}}$  and isolation  $I_{\text{bw}}$  are defined as

$$T_{\text{fw}} = \frac{CC_{\text{fw}}}{CC_{\text{in}}}, I_{\text{bw}} = 10 \log \frac{CC_{\text{in}}}{CC_{\text{bw}}} \quad (2)$$

here,  $CC_{\text{in}}$  is the coincidence counts of initial input photons. The calculated values of  $T_{\text{fw}}$ ,  $\mathcal{F}$  and  $I_{\text{bw}}$  for four polarization qubit states without any noise correction are presented in Table . It is very clear that we realize the high transmission and fidelity of polarization qubits in forward direction and the low transmission in backward direction.

Ultimately, we study the non-reciprocity of single photon storage process in our system. The non-reciprocity light storage has attracted many interests due to potential applications in asymmetric quantum networks, and it was demonstrated in a whispering-gallery-mode optical microresonator [44] based on Brillouin-scattering-induced transparency recently by using a coherent light as input. Here, we demonstrate a quantum non-reciprocal storage of a true single photon based on our non-reciprocity device.

We input single photons in forward and backward directions respectively with a fixed coupling laser. We block one path  $L$  of M-Z interferometer as shown in Fig.1(a). Note that the input signals (blue lines in Fig.4) in two propagation cases are the same when we take the overall loss of photons into account. In the forward propagation case, the dark state is formed leading to a high transparency of signal, which is the first step to realize single photon storage based on EIT storage protocol (see Method sections for more details). After we shut off the coupling adiabatically, the single photon is stored in the atomic ensemble. We utilize sequential coupling laser pulses to dynamically write and read the single photon schematically illustrated in the green line of Fig.4(a). The underlying mechanism in storage process can be considered as the conversion between atomic collective spin excitation and optical mode. After a programmed storage time, we read out the signal and the retrieved component of signal (red part in read out process) is depicted in Fig.4(a). Here, the  $OD$  of the atomic cloud 2 in storage process is set to be 54, and the storage efficiency is close to 9% which is mainly limited by the low  $OD$  of atoms in our system. The storage efficiency can be further improved by enlarging the  $OD$  of the atomic cloud 2 and by optimizing the input pulse wave packet to match the EIT



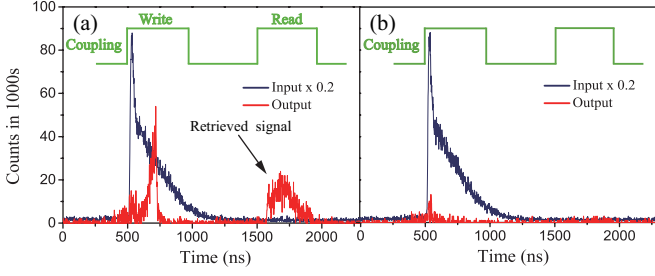


Figure 4. **The non-reciprocal quantum storage.** (a) The input signal (blue line) and stored signal (red line) before and after storage process in forward-propagation case. (b) The input signal (blue line) and output signal (red line) in backward-propagation case.

bandwidth of the atomic cloud 2. For comparison, we try the single photon storage in backward case as shown in Fig.4(b). It is obvious that we cannot observe a clear retrieved signal, implying a high isolation for backward-propagation signal. The forbidden storage process arises from the reason that optical modes cannot satisfy the condition of EIT process in backward-propagation.

In summary, we propose and experimentally demonstrate quantum non-reciprocity based on cold atomic ensembles. We exploit an asymmetric interaction between single photons and cold atoms to realize the non-reciprocity in our experiment. Besides, we realize the non-reciprocal transmission of polarization qubits and non-reciprocal quantum storage of a true single photon, which shows potential applications in quantum information processing. It is an outlook that this non-reciprocity mechanism would be realized by using single resonator enhanced atom [28] initially prepared in a specific Zeeman state like  $|g_{-2}\rangle$  in this work or integrated vapor cell [45], these could give prospective for future integrated quantum information processing.

## METHOD SECTIONS

**Preparation of a true single photon.** We generate heralded single photons through SFWM process in cold  $^{85}\text{Rb}$  atoms trapped in a 2D magneto-optical trap (MOT). The repetition rate of our experiment is 100 Hz and experimental window is 1.3 ms during which the MOT magnetic field is switched off completely. The pumps 1 and 2 are controlled by two AOMs modulated by arbitrary function generators (Tektronix, AFG3252). Two lenses each with a focal length of 500 mm are used to couple the signal fields S1 and S2 emitted from atomic cloud 1. The pumps 1 and 2 are collinear, and hence their respective signal fields are collinear to due to the phase matching condition  $k_{p1} - k_{S1} = k_{p2} - k_{S2}$  in the SFWM process, as in our previous work [46]. The two signal photons are ultimately collected into their respec-

tive single-mode fibers and are detected by two single photon detectors (avalanche diode, PerkinElmer SPCM-AQR-16-FC, 60 efficiency, maximum dark count rate of 25/s). The signals from the two detectors are then sent to a time-correlated single photon counting system (TimeHarp 260) to measure their time-correlated function.

## Asymmetric interaction between single photons and atoms

The optical properties of atomic system are fundamentally determined by their intrinsic energy-level configuration. In our work, the photons couple with specific atomic transitions, contributing to the direction-dependent transparency and absorption, inducing this non-reciprocity. The photons interactions with atoms in forward and backward directions become asymmetrical, the interaction Hamiltonian can be written as follow:

In forward-propagation case, the interaction Hamiltonian  $H_{\text{int}}^{\text{fw}}$  can be described as

$$H_{\text{int}}^{\text{fw}} = -\frac{\hbar}{2} \left( \sum_{i=-2}^2 \Omega_{pi}^+ |e_{i+1}\rangle \langle g_i| + \Omega_{ci}^+ |e_{i+1}\rangle \langle s_i| + \text{c.c.} \right) - \hbar \sum_{i=-2}^2 (\Delta\omega_p |e_{i+1}\rangle \langle e_{i+1}| + \delta |s_i\rangle \langle s_i|) \quad (3)$$

here,  $|g_i\rangle$  refer to the Zeeman states of level  $g$ , where  $-F \leq i \leq F$ . The similar definitions are adapted to levels  $s$  and  $e$ .  $\Omega_{pi}^+ = -\mu_{e_{i+1},g_i} E_p^+ / \hbar$  and  $\Omega_{ci}^+ = -\mu_{e_{i+1},s_i} E_c^+ / \hbar$  denote the Rabi frequencies of  $\sigma^+$  photons and coupling laser respectively.  $\mu_{e_{i+1},g_i}$  represents the dipole moment between Zeeman states  $|e_{i+1}\rangle$  and  $|g_i\rangle$ .  $\Delta\omega_p = \omega_p - \omega_{ge}$  is the single-photon detuning,  $\delta = \Delta\omega_p - \Delta\omega_c$  represents the two-photon detuning.

Furthermore, in backward-propagation case, the interaction Hamiltonian  $H_{\text{int}}^{\text{bw}}$  can be written as

$$H_{\text{int}}^{\text{bw}} = -\frac{\hbar}{2} \left[ \sum_{i=-1}^2 (\Omega_{pi}^- |e_{i-1}\rangle \langle g_i| + \Omega_{ci}^+ |e_{i-1}\rangle \langle s_{i-2}|) + \Omega_{p-2}^- |e_{-3}\rangle \langle g_{-2}| + \text{c.c.} \right] - \hbar \sum_{i=-1}^2 (\Delta\omega_p |e_{i-1}\rangle \langle e_{i-1}| + \delta |s_{i-2}\rangle \langle s_{i-2}|) - \hbar \Delta\omega_p |e_{-3}\rangle \langle e_{-3}| \quad (4)$$

$\Omega_{pi}^- = -\mu_{e_{i-1},g_i} E_p^- / \hbar$  represents the Rabi frequency of  $\sigma^-$  photons.

The respective susceptibility  $\chi_{fw(bw)}$  can be formula as [42]

$$\chi_{fw} = -\frac{2N}{5\hbar\epsilon_0} \sum_{i=-2}^2 \frac{|\mu_{e_{i+1},g_i}|^2}{\Omega_{pi}^+} \rho_{g_i,e_{i+1}} \quad (5)$$

$$\chi_{bw} = -\frac{2N}{5\hbar\epsilon_0} \left( \sum_{i=-1}^2 \frac{|\mu_{e_{i-1},g_i}|^2}{\Omega_{p_i}^-} \rho_{g_i,e_{i-1}} + \frac{|\mu_{e_{-3},g_{-2}}|^2}{\Omega_{p_{-2}}^-} \rho_{g_{-2},e_{-3}} \right) \quad (6)$$

here,  $N$  is atomic density. The density matrix  $\rho_{g_i,e_{i+1}}$  can be calculated from master equation

$$\frac{\partial \rho}{\partial t} = -\frac{i}{\hbar} [H_{int}, \rho] - \frac{1}{2} \{\Gamma, \rho\} \quad (7)$$

Ultimately, susceptibility  $\chi_{fw(bw)}$  can be written as

$$\chi_{fw} = \frac{N}{5\hbar\epsilon_0} \sum_{i=-2}^2 \frac{4|\mu_{e_{i+1},g_i}|^2 (\delta + i\gamma_{gs})}{|\Omega_{ci}^+|^2 - 4(\delta + i\gamma_{gs})(\Delta\omega_p + i\gamma_{ge})} \quad (8)$$

$$\chi_{bw} = \frac{N}{5\hbar\epsilon_0} \left( \sum_{i=-1}^2 \frac{4|\mu_{e_{i-1},g_i}|^2 (\delta + i\gamma_{gs})}{|\Omega_{ci}^+|^2 - 4(\delta + i\gamma_{gs})(\Delta\omega_p + i\gamma_{ge})} - \frac{|\mu_{e_{-3},g_{-2}}|^2}{\Delta\omega_p + i\gamma_{ge}} \right) \quad (9)$$

We consider an effective  $OD = NLk_0 |\mu_{e,g}|^2 / (\epsilon_0 \gamma_{ge} \hbar)$ ,  $\mu_{e,g}$  is the effective dipole moments. Moreover, we take into account different Clebsch-Gordan coefficients of various transitions between different Zeeman sublevels and the relations between  $\mu_{e,g}$  and  $\mu_{e_{i+1},g_i} (\mu_{e_{i-1},g_i})$  referred to [47].  $k_0$  is the wave vector,  $L$  is the length of atomic cloud,  $\gamma_{gs}, \gamma_{ge}$  are the mean dephasing rates of atomic transition  $|g\rangle \rightarrow |s\rangle$  and  $|g\rangle \rightarrow |e\rangle$  respectively.

We observe an asymmetric permittivity in forward and backward propagation cases, which induces the non-reciprocity in our scheme. The transmission for forward  $T_{fw}$  and backward  $T_{bw}$  propagation cases can be described by

$$T_{fw(bw)} = e^{-2\text{Im}[(\omega_p/c)(1+\chi_{fw(bw)}/2)]L} \quad (10)$$

here,  $\omega_p$  is the frequency of photon,  $c$  is the speed of light in vacuum.

**Quantum state tomography of qubits.** To characterize the output polarization qubit state, we project single photon states onto four bases  $|H\rangle, |V\rangle, (|H\rangle + i|V\rangle)/\sqrt{2}$  and  $(|H\rangle + |V\rangle)/\sqrt{2}$  by a polarization analyzer consisting of a QWP, HWP and PBS. Then, we obtain a set of data for reconstructing the density matrix. The fidelity is calculated by the formula  $\mathcal{F} = \text{Tr}(\sqrt{\sqrt{\rho}\rho_{\text{ideal}}\sqrt{\rho}})^2$ , which compares the reconstructed density matrix  $\rho$  with ideal density matrix  $\rho_{\text{ideal}}$ . Ultimately, we evaluate the standard deviation in our experiment by the Poisson statistics using Monte Carlo simulation with assistance of Mathematica software.

**EIT quantum memory.** In the forward-propagation case, after propagating through a 200-m optical fiber (corresponding to a time delay of  $\sim 1 \mu\text{s}$ ), S2 photon is focus onto the atomic cloud 2 by using a lens with focus length of 300 mm. We adiabatically switch off the coupling laser, and a stored atomic collective excitation is obtained given by  $1/\sqrt{m} \sum e^{ik_S \cdot r_i} |g\rangle_1 \cdots |s\rangle_i \cdots |g\rangle_m$  [48], also called as a spin wave.  $k_S = k_c - k_{s2}$  is the wave vector of atomic spin wave,  $k_c$  and  $k_{s2}$  are the vectors of coupling and S2 fields,  $r_i$  denotes the position of the  $i$ -th atom in atomic cloud 2. After a programmed storage time, the spin wave is converted back into photonic excitation by switching on the coupling laser again.

**Author contributions** M.X.D conceived the idea with discussions with D.S.D. and B.S.S.. M.X.D carried out the experiments with assistance from D.S.D., W.H.Z. and Y.C.Y.. All authors contributed to the discussions and analysis of results. M.X.D. and D.S.D. wrote the manuscript with contributions from B.S.S.. D.S.D., B.S.S. and G.C.G. supervised the project.

**Competing financial interests** The authors declare no competing financial interests.

**Acknowledgments** The authors thank Prof. Chun-Hua Dong, Dr. Wei Zhang, and Dr. Meng-Jun Hu for fruitful discussions. This work was supported by National Key R&D Program of China (2017YFA0304800), the National Natural Science Foundation of China (Grant Nos. 61525504, 61722510, 61435011, 11174271, 61275115, 11604322), and the Innovation Fund from CAS, Anhui Initiative in Quantum Information Technologies (AHY020200), the Fundamental Research Funds for the Central Universities, and the Youth Innovation Pro motion Association of CAS under Grant No. 2018490.

\* dds@ustc.edu.cn

† drshi@ustc.edu.cn

- [1] J. I. Cirac, P. Zoller, H. J. Kimble, and H. Mabuchi, *Physical Review Letters* **78**, 3221 (1997).
- [2] P. Lodahl, S. Mahmoodian, S. Stobbe, A. Rauschenbeutel, P. Schneeweiss, J. Volz, H. Pichler, and P. Zoller, *Nature* **541**, 473 (2017).
- [3] S. Fan, R. Baets, A. Petrov, Z. Yu, J. D. Joannopoulos, W. Freude, A. Melloni, M. Popović, M. Vanwolleghem, D. Jalas, *et al.*, *science* **335**, 38 (2012).
- [4] D. Jalas, A. Petrov, M. Eich, W. Freude, S. Fan, Z. Yu, R. Baets, M. Popović, A. Melloni, J. D. Joannopoulos, *et al.*, *Nature Photonics* **7**, 579 (2013).
- [5] Z. Yu and S. Fan, *Nature photonics* **3**, 91 (2009).
- [6] M. S. Kang, A. Butsch, and P. S. J. Russell, *Nature Photonics* **5**, 549 (2011).
- [7] N. A. Estep, D. L. Sounas, J. Soric, and A. Alù, *Nature Physics* **10**, 923 (2014).
- [8] D. L. Sounas, C. Caloz, and A. Alu, *Nature communications* **4**, 2407 (2013).
- [9] H. Lira, Z. Yu, S. Fan, and M. Lipson, *Physical review*

- letters **109**, 033901 (2012).
- [10] L. D. Tzuang, K. Fang, P. Nussenzeig, S. Fan, and M. Lipson, *Nature photonics* **8**, 701 (2014).
  - [11] L. Fan, J. Wang, L. T. Varghese, H. Shen, B. Niu, Y. Xuan, A. M. Weiner, and M. Qi, *Science* **335**, 447 (2012).
  - [12] N. Bender, S. Factor, J. D. Bodyfelt, H. Ramezani, D. N. Christodoulides, F. M. Ellis, and T. Kottos, *Physical review letters* **110**, 234101 (2013).
  - [13] L. Chang, X. Jiang, S. Hua, C. Yang, J. Wen, L. Jiang, G. Li, G. Wang, and M. Xiao, *Nature photonics* **8**, 524 (2014).
  - [14] B. Peng, Ş. K. Özdemir, F. Lei, F. Monifi, M. Gianfreda, G. L. Long, S. Fan, F. Nori, C. M. Bender, and L. Yang, *Nature Physics* **10**, 394 (2014).
  - [15] M. Hafezi and P. Rabl, *Optics express* **20**, 7672 (2012).
  - [16] X.-W. Xu and Y. Li, *Physical Review A* **91**, 053854 (2015).
  - [17] S. Manipatruni, J. T. Robinson, and M. Lipson, *Physical review letters* **102**, 213903 (2009).
  - [18] Z. Shen, Y.-L. Zhang, Y. Chen, C.-L. Zou, Y.-F. Xiao, X.-B. Zou, F.-W. Sun, G.-C. Guo, and C.-H. Dong, *Nature Photonics* **10**, 657 (2016).
  - [19] F. Ruesink, M.-A. Miri, A. Alu, and E. Verhagen, *Nature communications* **7**, 13662 (2016).
  - [20] K. Fang, J. Luo, A. Metelmann, M. H. Matheny, F. Marquardt, A. A. Clerk, and O. Painter, *Nature Physics* **13**, 465 (2017).
  - [21] E. Verhagen and A. Alù, *Nature Physics* **13**, 922 (2017).
  - [22] D.-W. Wang, H.-T. Zhou, M.-J. Guo, J.-X. Zhang, J. Evers, and S.-Y. Zhu, *Physical review letters* **110**, 093901 (2013).
  - [23] J.-H. Wu, M. Artoni, and G. La Rocca, *Physical review letters* **113**, 123004 (2014).
  - [24] S. Horsley, J.-H. Wu, M. Artoni, and G. La Rocca, *Physical review letters* **110**, 223602 (2013).
  - [25] B. Megyeri, G. Harvie, A. Lampis, and J. Goldwin, *Physical review letters* **121**, 163603 (2018).
  - [26] K. Xia, F. Nori, and M. Xiao, *Physical review letters* **121**, 203602 (2018).
  - [27] M. Scheucher, A. Hilico, E. Will, J. Volz, and A. Rauschenbeutel, *Science* **354**, 1577 (2016).
  - [28] C. Sayrin, C. Junge, R. Mitsch, B. Albrecht, D. O'Shea, P. Schneeweiss, J. Volz, and A. Rauschenbeutel, *Physical Review X* **5**, 041036 (2015).
  - [29] I. Söllner, S. Mahmoodian, S. L. Hansen, L. Midolo, A. Javadi, G. Kiršanskė, T. Pregnolato, H. El-Ella, E. H. Lee, J. D. Song, *et al.*, *Nature nanotechnology* **10**, 775 (2015).
  - [30] K. Xia, G. Lu, G. Lin, Y. Cheng, Y. Niu, S. Gong, J. Twamley, *et al.*, *Physical Review A* **90**, 043802 (2014).
  - [31] S. Zhang, Y. Hu, G. Lin, Y. Niu, K. Xia, J. Gong, and S. Gong, *Nature Photonics* **12**, 744 (2018).
  - [32] E. Knill, R. Laflamme, and G. J. Milburn, *nature* **409**, 46 (2001).
  - [33] L. Zhou, Z. Gong, Y.-x. Liu, C. Sun, F. Nori, *et al.*, *Physical review letters* **101**, 100501 (2008).
  - [34] L. Zhou, L.-P. Yang, Y. Li, C. Sun, *et al.*, *Physical review letters* **111**, 103604 (2013).
  - [35] L. Tang, J. Tang, W. Zhang, G. Lu, H. Zhang, Y. Zhang, K. Xia, and M. Xiao, *Physical Review A* **99**, 043833 (2019).
  - [36] J.-T. Shen and S. Fan, *Physical review letters* **95**, 213001 (2005).
  - [37] Z. Wang, L. Du, Y. Li, and Y.-x. Liu, *arXiv preprint arXiv:1905.04888* (2019).
  - [38] D. E. Chang, A. S. Sørensen, E. A. Demler, and M. D. Lukin, *Nature Physics* **3**, 807 (2007).
  - [39] V. Balić, D. A. Braje, P. Kolchin, G. Yin, and S. E. Harris, *Physical review letters* **94**, 183601 (2005).
  - [40] S. Du, J. Wen, and M. H. Rubin, *JOSA B* **25**, C98 (2008).
  - [41] Y.-C. Chen, C.-W. Lin, and A. Y. Ite, *Physical Review A* **61**, 053805 (2000).
  - [42] B. Wang, S. Li, J. Ma, H. Wang, K. Peng, and M. Xiao, *Physical Review A* **73**, 051801 (2006).
  - [43] V. Tiwari, S. Singh, H. Rawat, M. P. Singh, and S. Mehendale, *Journal of Physics B: Atomic, Molecular and Optical Physics* **43**, 095503 (2010).
  - [44] C.-H. Dong, Z. Shen, C.-L. Zou, Y.-L. Zhang, W. Fu, and G.-C. Guo, *Nature communications* **6**, 6193 (2015).
  - [45] T. Overstolz, J. Haesler, G. Bergonzi, A. Pezous, P.-A. Clerc, S. Ischer, J. Kaufmann, and M. Despont, in *2014 IEEE 27th International Conference on Micro Electro Mechanical Systems (MEMS)* (IEEE, 2014) pp. 552–555.
  - [46] D.-S. Ding, Z.-Y. Zhou, B.-S. Shi, and G.-C. Guo, *Nature communications* **4**, 2527 (2013).
  - [47] D. A. Steck, “Rubidium 85 d line data,” (2001).
  - [48] M. Fleischhauer and M. D. Lukin, *Physical Review Letters* **84**, 5094 (2000).